Nanoscale

Accepted Manuscript

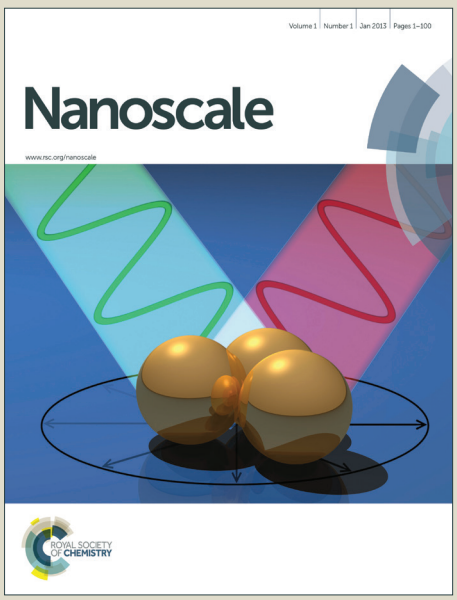

ROYAL SOCIETY OF CHEMISTRY

www.rsc.org/nanoscale

Journal Name

RSCPublishing

ARTICLE

Accurate hierarchical control of hollow crossed $NiCo_2O_4$ nanocubes for superior lithium storage

Cite this: DOI: 10.1039/x0xx00000x

Hong Guo*, Lixiang Liu, Tingting Li, Weiwei Chen, Jiajia Liu, Yuanyuan Guo and Yicheng Guo

Received 00th January 2012,
Accepted 00th January 2012

DOI: 10.1039/x0xx00000x

www.rsc.org/

An effective approach of simultaneous coordinating etching and precipitating reaction is employed to prepare hollow crossed $NiCo_2O_4$ nanocubes as anode materials for Li-ion batteries. Amorphous hollow $(NiCo_x)O(OH)$ nanoboxes form uniformly firstly, and the subsequent calcination results in the formation of $NiCo_2O_4$ nanocubes. It exhibits a stable reversible capacity of 1160 $mAhg^{-1}$ at constant current density of 200 mAg^{-1}, and capacity retention keeps over 91.1% after 200 cycles. The unique hollow structure can shorten the length of Li-ion diffusion, which is benefit for the rate performance. Furthermore, the hollow structure offers a sufficient void space, which sufficiently alleviates the mechanical stress caused by volume change. Additionally, the multi-elements characteristics of active materials allow the volume change to take place in a stepwise manner. Therefore, the hollow crossed $NiCo_2O_4$ nanocube electrode exhibits excellent electrochemical performance. This strategy method is simple, low cost, which may shed light on a new avenue for fast synthesis of hollow crossed structural nano functional materials for energy storage, catalyst, sensor and other new applications.

Introduction

The development of accurate designing molecular architecture of nano/micro-materials is one of central tasks of modern science and technology due to the fascinating properties are most dependent on its structure, such as size, morphology and component.[1-4] Most recently, many efforts have been focused on work related to design and regulate advanced materials with hollow structures due to well-defined interior voids, high specific surface area, low density, accommodate volume change without pulverizing compared with that of solid counterparts of the same size,[5-9] and thus they have attracted much attention in a diverse range of applications such as drug delivery, environmental remediation, energy storage and various new applications.[7-14] Especially, the novel hollow mixed metal oxides containing multiple functional component exhibit enhanced performance in the field of energy and environmental science compared to single component hollow structures.[15-19] For example, Teng and co-workers obtained Mn_3O_4-Co_3O_4 hollow spheres, which have a higher catalytic activity for CO oxidation than single Co_3O_4 ones.[20] Our previous prepared hollow cage-bell Ag@TiO_2 materials exhibit enhanced lithium-ion storage.[21] Lou and co-workers synthesized hollow $CoSnO_3$@C microcubes and hollow $CoMn_2O_4$ nanoboxes with highly reversible lithium storage.[22,23]

Transition metal oxides (TMO), especially nickel cobaltite, a type of spinel oxide, has attracted considerable interest as high capacity anode materials for LIBs.[24-26] However, those elctrodes suffers severe mechanical disintegration due to the drastic volumetric changes during lithium ion insertion and extraction, and therefore leads to rapid deterioration in capacity. To solve this problem, allowing the electrochemical reaction to proceed in a hybrid matrix of distinct material systems, such as the oxides and carbonaceous materials.[23] In this case, the confining matrix, which can be either active or inactive towards lithium, may be results in the volume change occurs in a step-wise manner rather than at a certain fixed potential, and thus the unreacted component can accommodate the strain yielded by the reacted phase. Futhermore, the coupling of two metal species could render the TMOs with rich redox reactions and improve electronic conductivity. Additionally, the various combinations of the cations in the TMOs provide vast opportunities to manipulate the physical/chemical properties. As a result, the geometric configuration and cycling stability of electrode are improved. Therefore, ternary $NiCo_2O_4$ exhibits higher electrical conductivity and improves electrochemical activity compared with binary metal oxides NiO and Co_3O_4.[27-29] However, there are only a few reports on the application of $NiCo_2O_4$ as an anode material for LIBs. Another popular way to improve the electrochemical performance of TMOs has been focused on controlling the volumetric change by using small particles with various morphologies including nanotube, nanowall, nanosheet, nanobowl, nanocone, and porous solid, of which hollow particles are of particular interest for reversible lithium ion storage because of their short Li^+ diffusion and good toleration for volume change during cycling.[30-34] Though these procedures are effective, each design strategy alone always leads to limited improvement in the electrochemical properties of TMOs. And thus, the development of a facile, scalable and controllable fabrication of durable hybrid TMOs

materials with satisfactory cycling ability and high capacity is still highly desirable for LIBs. Besides, to our best knowledge, reports on the fast synthesis of hollow crossed structural TMOs are quite rare compared with current methods that produced nanostructure, and can be an advantage for chemists to elaborate possible new constructions from all chemical components without any time-restricted conditions.

Herein, we chose Ni-Co-O to demonstrate our concept and propose a facile fast strategy to prepare hollow crossed $NiCo_2O_4$ nanocubes as illustrated in Scheme 1. The as-prepared crossed nanocube is hired as the template, and then $S_2O_3^{2-}$ is used to self-gather around and coordinating etching of Cu_2O. Subsequently, OH^- originated from hydrolysis of $S_2O_3^{2-}$ results of the precipitation of Ni and Co ions, and thus $(NiCo_x)O(OH)$ precursor formed. Finally, thermal treatment facilitate the products of hollow crossed $NiCo_2O_4$ nanocubes. The two active components of Ni and Co oxides can realize the high capacity feature of electrode and can make the volume change of electrode take place in a stepwise manner due to the different lithiation potentials of two active components, leading to a stable cycling performance. Meanwhile, compared with conventional methods produced metal oxides nano electrodes, the hollow crossed nanocubes prepared as such have relatively high surface area and a stable hollow configuration without the destructive effect of template removal on product morphology. The former can render much contact area between active components and Li ions in the process of electrochemical reaction, while the latter one may help the electrode to accommodate large volume change without pulverizing. Futhermore, the hollow structures can short ionic/electronic diffusion length and provide efficient channels for mass transport. So, the high specific capacity and good cycling performance can be expected.

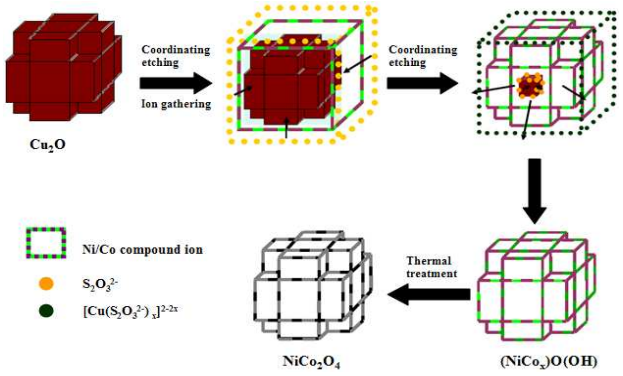

Scheme 1. Representative illustration of the formation of hollow crossed $NiCo_2O_4$ nanocubes by simultaneous coordinating etching of Cu_2O nanocubes.

Experimental

Preparation of solid Cu_2O crossed nanocubes

In a typical synthesis, 5 mL of aqueous solution of $CuCl_2$ (0.2 M), 5 mL of aqueous solution of PVP K30 (0.2 g)was added into 55 mL of deionized water under stirring, after 10min, 10 mL of a mixture solution containing Na_2CO_3 (1 M) and potassium citrate (0.6 M) was added into light blue solution, then the solution color turned into dark blue and placed into a 100 mL Teflon cup. The autoclave was heated to 80 °C for 2 h. The resulting red product was harvested by several rinse-precipitation cycles with deionized (DI) water for further characterization.

Preparation of amorphous $(NiCo_x)O(OH)$ crossed nanoboxes

Cu_2O templates (10.0 mg), $CoCl_2{\cdot}6H_2O$ (0.04 mmol), $NiCl_2{\cdot}6H_2O$ (0.02 mmol) were added into the ethanol/water mixed solvent (10.0 mL, volume ratio = 1:1) with the present of PVP K30(1.65g) under stirring, the reaction temperature was controlled and set to 60 ℃ for 10min，followed by dropwise addition of 4 mL of aqueous solution of $Na_2S_2O_3$ (1 M) and the reaction was lasted for 10 min at ambient conditions until the color of suspension solution changed from red to purple. Eventually, the resulting product $(NiCo_x)O(OH)$ was harvested by several rinse-centrifugation cycles with deionized water and ethanol, and finally dried at room temperature for further characterization.

Synthesis of hollow $NiCo_2O_4$ crossed nanoboxes

Certain amount of $(NiCo_x)O(OH)$ nanoboxes was successively annealed in Ar flowing at 400 °C for 4 h with a slow ramp rate of 1 °C min^{-1} to make the hollow $NiCo_2O_4$ crossed nanoboxes.

Characterization

X-ray diffraction (XRD) was carried out to identify the phase composition of synthesized samples over the 2θ range from 20° to 90° using a Rigaku D/max-A diffractometer with Co Kα radiation. A Fourier transform infrared spectroscope (FTIR, Themo Nicolet 670FT-IR) was used for recording the FTIR spectra of the sample ranging from 400 to 4000 cm^{-1}. Morphologies of the synthesized samples were observed with a AMRAY 1000B scanning electron microscope (SEM), and the microstructural characteristics of samples were observed by high-resolution transmission electron microscope (HR-TEM, JEOL JEM-2010) working at 200 kV accelerating voltage and the lattice structure was identified by selected area electron diffraction (SAED) technique. Nitrogen adsorption-desorption measurements were conducted at 77 K on a Micromeritics Tristar apparatus. Specific surface areas were determined following the Brunauer-Emmet-Teller analysis.

Electrochemical Measurements

For electrochemical performance evaluation, half-cell studies were performed. In the experimental electrode, acetylene black powder and polyvinylidene fluoride (PVDF) were used as conductive additive and binder. The synthesized active materials were mixed with acetylene black and PVDF dissolved in N-methyl-pyrrolidinone in the weight ratio of 80:10:10 to form slurry, which was painted on a copper foil used as current collector. After solvent evaporation, the electrode was pressed and dried at 120℃ under vacuum for 48 h. The cells were assembled in argon filled glove-box. Metallic lithium foil was used as counter electrode. The electrolyte was 1M $LiPF_6$ in a mixture of ethylene carbonate (EC) and dimethyl carbonate (DMC) (1:1 in vol. ratio). Cycling tests were carried out at the charge and discharge current density of 100 mAg^{-1}, in the voltage range of 0.01–3.0 V versus Li/Li^+ by Land 2100A tester. Cyclic voltammetry was performed between 0.01 and 3.0 V with scan rate of 0.01 mVs^{-1}.

Results and discussion

Structure and morphology of hollow crossed $NiCo_2O_4$ nanocubes

The XRD patterns of the synthesized materials and its precursor, shown in Fig. 1a, declare the product after calcinations at 400℃ exhibits a higher crystallinity than that of $(NiCo_x)O(OH)$ precursor. The samples exhibit diffraction lines which can be assigned to the

spinel $NiCo_2O_4$, and no other peaks are identified, indicating the samples are a single phase of spinel with good phase purity. The unit cell dimension of the spinel structure was determined from the observed d-spacings for the (2 2 0) and (3 1 1) planes. The calculated a value (0.8011 nm) of the sample is much close to 0.8114 nm corresponding to spinel structure $NiCo_2O_4$ (JCPDS card no. 73-1702). Detailed analysis of the peak broadening of the (3 1 1) reflection of $NiCo_2O_4$ using the Scherrer equation indicates an average crystallite size ca. 6 nm, suggesting that these $NiCo_2O_4$ particles are composed of nanocrystal subunits. The FTIR spectrum images of the prepared hollow $NiCo_2O_4$ crossed nanocubes and that of the precursor are shown in Fig. 1b. The broad absorption peaks centered at ca. 3493 is associated with the asymmetric and symmetric stretching vibrations of the -OH group of absorbed water molecules, and that at 1552 cm^{-1} is assigned to the bending vibrations of the water molecules. The broad absorption peaks ranged of 500-1000 cm^{-1} are assigned to metal-O bond.[35] The peak intensity of metal-O bond for the sample is different from that of precursor, implying the structure of prepared sample has a little discrepancy with its precursor.

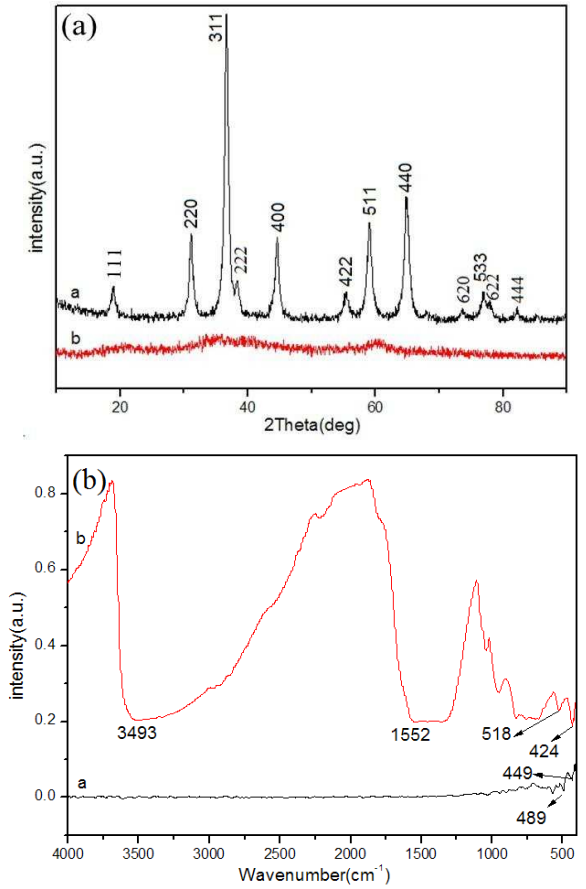

Fig. 1 (a) XRD pattern and (b) FTIR spectra of hollow crossed $NiCo_2O_4$ nanocubes and its precursor corresponding to curve a and b, respectively.

SEM images of the prepared Cu_2O and hollow $NiCo_2O_4$ crossed nanocubes yielded by calcinations at 400 ℃ at different magnifications are shown as Fig. 2a-c. It is obvious that the synthesized $NiCo_2O_4$ samples maintain the morphology of prepared Cu_2O except for a little shrinkage in size, which are crossed nanocube ca. 500 nm uniformly. The $NiCo_2O_4$ is hollow crossed nanocube structure, as evidenced by the mesospheres as Fig. 2b and c. Observation on part particles with partially broken shell, as shown in Fig. 2c indicates that the thickness of shell is estimated to ca. 30-50 nm and the surface of the synthesized $NiCo_2O_4$ powder is made up from nano-sized small particles. The cleft of these nanoboxes might be caused by rapid mass-transport across the shells during fast dissolution of the Cu_2O. The unique hollow crossed morphology of $NiCo_2O_4$ nanocube is also characterized by TEM and HR-TEM, as illustrated in Fig. 2d-f. The low-magnification TEM image in Fig. 2d shows a hollow crossed nanocube, which is a visible hollow interior structure obviously. Especially, a typical nanobox with well-defined interior and very thin shell can be detected as Fig. 2e, which is in good agreement with SEM analysis. The thin thickness of shell of nanocubes is ca. 40 nm. Its selected-area electron diffraction (SAED) pattern (Fig. 2e inset) reveals the diffraction rings 1-3 are indexed to (3 1 1), (4 0 0), and (5 1 1) diffraction of spinel structure $NiCo_2O_4$, respectively. Additionally, HRTEM micrograph (Fig. 2f) of the part of sample also detects the lattice spacing (0.248 nm) agrees with (3 1 1) plane spacing of cubic $ZnCo_2O_4$ with a spinel structure, which is in agreement with XRD results.

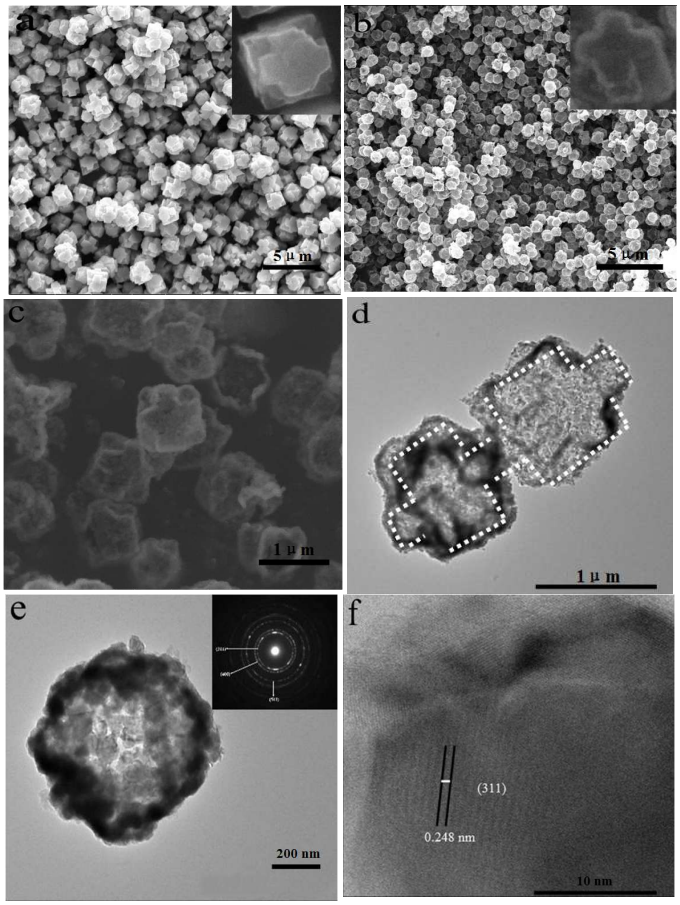

Fig. 2 SEM image of prepared Cu_2O crossed nanocubes (a). SEM images (b, c), TEM (d, e) images, HRTEM micrographs (e) and selected area electron diffraction (f) of as-synthesized hollow crossed $NiCo_2O_4$ nanocubes yielded by calcinations at 400 ℃**.** The inset in (e) is the selected area electron diffraction (SAED).

The N_2 adsorption/desorption isotherms and the pore size distribution of the obtained hollow $NiCo_2O_4$ crossed nanocubes are shown as Fig. 3, The isotherms are identified as type IV, which is the characteristic isotherm of mesoporous materials. The pore size distribution data indicates that average pore diameters of the product

are in the range of 4.5-7.8 nm. The BET surface area of the sample is 82.25 m^2g^{-1}. The single-point total volume of pores at $P/P_0 = 0.975$ is 0.242 cm^3g^{-1}.These indicate that the prepared samples have a loose mesoporous structure. This structure not only can keep the nano effect of active components but also help to buffer the volume changes of hollow $NiCo_2O_4$ crossed nanocubes electrode during electrochemical reaction.

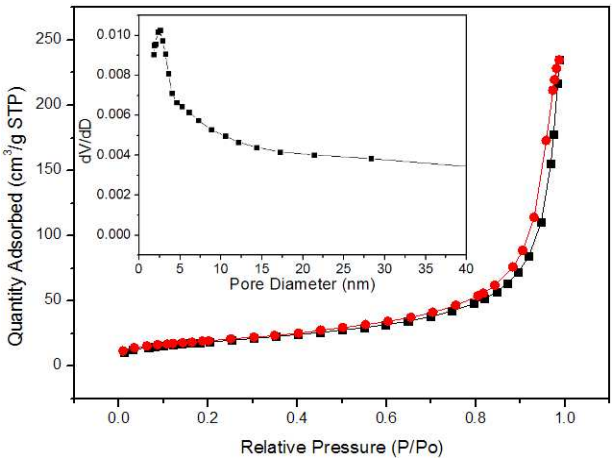

Fig. 3 Nitrogen adsorption/desorption isotherm and Barrett-Joyner-Halenda (BJH) pore size distribution plot (inset) of the prepared hollow crossed $NiCo_2O_4$ nanocubes.

Synthesis mechanism of hollow $NiCo_2O_4$ crossed nanocubes with controlled morphologies.

The formation mechanism can be described as schematically illustrated in Scheme 1 by the following formula:

$$Cu_2O + XS_2O_3^{2-} + H_2O \longrightarrow [Cu_2(S_2O_3)_x]^{2-2x} + 2OH^- \quad (1)$$

$$S_2O_3^{2-} + H_2O \longleftrightarrow HS_2O_3^- + OH^- \quad (2)$$

$$2Ni^{2+} + 2XCo^{2+} + 2OH^- + O_2 \longrightarrow 2(NiCo_X)O(OH) \quad (3)$$

$$(NiCo_x)O(OH) \longrightarrow NiCo_2O_4 + H_2O \quad (4)$$

$S_2O_3^{2-}$ can achieve selective erosion for Cu^{2+} effectively which in the mixed solution of Co^{2+}, Ni^{2+} and Cu^{2+} on the basis of Pearson's hard and soft acid-base (HSAB) principle. Firstly, coordinating etching reaction of $S_2O_3^-$ to crossed Cu_2O nanocubes was taken place under ambient conditions from its out to core, and offered OH^- as Equ. 1. At the same time, those OH^- originated from hydrolysis of excess $S_2O_3^-$ (Equ. 2) can make the precipitation of Co and Ni ions (Equ. 3). And thus the Ni^{2+} and Co^{2+} around with etching interface of Cu_2O are self-gather and precipitate in aqueous solution with high concentration of OH^-, which process results in the formation of the shell of amorphous $(NiCo_x)O(OH)$ precursor. The shell of $(NiCo_x)O(OH)$ potentially thickens according to the concentration of Ni and Co ions with the proceeding of reaction as Equ.3. It is interesting that the dissolution process of Cu_2O also undergoes even the $(NiCo_x)O(OH)$ shell fully forms. The process is tracked to investigate according to Fig. 4a-f, which is SEM image of simultaneous coordinating etching of crossed Cu_2O nanocubes at 60 ℃ from 0 to 30 min. Compared with Fig. 2, the simultaneous coordinating etching products mirror closely that the final product was formed after calcination. It is found that clearly crossed structures can be detected initially (Fig. 4a). While the reaction is conducted for 5 min (Fig. 4b), the surface of sample becomes a little coarse and was transformed into hollow ones gradually. With the increase of reaction time (Fig. 4c, 10 min), the hollow crossed structures become more significantly. Further prolonging the reaction time, the interior of the nanocubes change empty as shown in Fig. 4d (15 min) and Fig. 4e, (20 min). Finally, the hollow crossed nanocubes are broken gradually, such as Fig. 4f (30 min). The reaction runs much fast, which dynamic process is different from the traditional concept of the sacrificial-template. Finally, $NiCo_2O_4$ crossed nanoboxes are obtained by thermal-induced dehydration of $(NiCo_x)O(OH)$ (Equ. 4), after annealing in Ar atmosphere. Compared with the method reported $NiCo_2O_4$ materials[29, 36-41], our strategy provides a novel route to prepare hollow crossed nanacubes with shorter time, more larger quantity, and lower cost. This rout can also be used to prepare other cage-bell advanced materials, such as TiO_2 (Fig. S1), CeO_2 (Fig. S2) and NiO (Fig. S3), for details see supporting information**.**

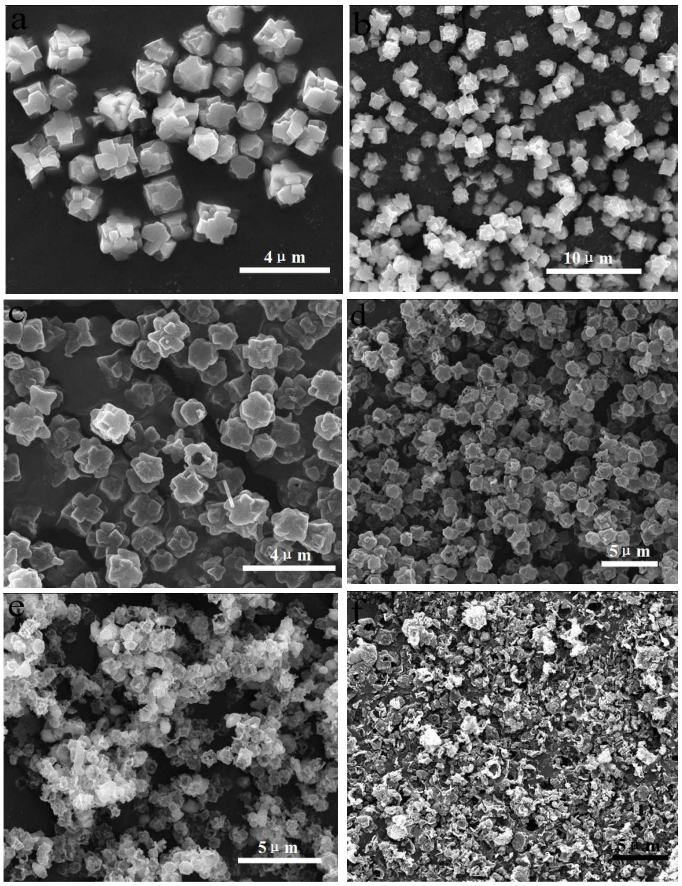

Fig. 4 SEM images of $(NiCo_x)O(OH)$ precursors by simultaneous coordinating etching of crossed Cu_2O nanocubes at 70 ℃ for 0 min (a), 5 min(b), 10 min (c), 15 min (d), 20 min, and 30 min (f).

Electrochemical characterizations of hollow $NiCo_2O_4$ crossed nanocubes

The electrochemical performance of the prepared hollow $NiCo_2O_4$ crossed nanocubes used for Li-ion anodic materials is investigated. According to Fig. 5a, the increase in cycling stability and capacity with the increase of reaction time from 5 min to 10 min is mainly attributable to the formation of hollow crossed structures. However, when the reacted time arrived at 30 min, its capacity fades drastically from 1203 to 156 $mAhg^{-1}$ after 100 cycles. This result is understandable because of the hollow structures are destroyed in the process of coordinating etching reaction according to Fig. 4. And

thus easy to cause pulverization of the electrode material in the process of charging and discharging.[33] The charge/discharge and cycle CV curves of hollow $NiCo_2O_4$ crossed nanocubes (10 min) electrode are shown in Fig. 5b and 5c, respectively. The anodic peak centered at 1.32 V can be assigned to the destruction of the $NiCo_2O_4$ crystal structure. The intense peak located at 0.95 V can be result from the reduction of Co and Ni ions to metallic Co and Ni, respectively. The cathodic peak centered at about 0.73 V corresponds to the formation of a SEI layer. According to the 1st, 2nd, and 200th discharge (Li^+ insertion) and charge (Li^+ extraction) curves at a current density of 100 mA g^{-1} in the voltage window of 0.01–3 V. There is a wide, steady discharging plateau at 0.95 V in the first cycle, followed by a gradual voltage decrease. The initial discharge and charge capacities are 1360 and 1161 $mAhg^{-1}$, respectively. The initial capacity loss is 199 $mAhg^{-1}$, which should be attributed to the formation of solid electrolyte interphase (SEI) and the reduction of metal oxide to metal with Li_2O formation. The initial coulombic efficiency is 85.3%, which is lower than most reported Ni and Co oxide electrodes.[42-45] These results are consistent with CV analysis. From the second cycle onwards, the long potential plateau was replaced by a long slope between 1.0 and 0.70 V. After 200 cycles, the capacity can also be kept at 1058 $mAhg^{-1}$, showing the excellent reversibility of electrode. The electrochemical reactions involved in the discharge and charge processes are believed to proceed as follows[46–50]:

$$NiCo_2O_4 + 8Li^+ + 8e^- \longrightarrow 2Co + Ni + 4Li_2O \quad (5)$$

$$Ni + Li_2O \longleftrightarrow NiO + 2Li^+ + 2e^- \quad (6)$$

$$Co + Li_2O \longleftrightarrow CoO + 2Li^+ + 2e^- \quad (7)$$

$$NiO + 2Li^+ \leftrightarrow Li_2O + Ni\text{-}2e \quad (8)$$

$$CoO + 1/3Li_2O \longleftrightarrow 1/3Co_3O_4 + 2/3Li^+ + 2/3e^- \quad (9)$$

To investigate electrochemistry performance under the different rate discharge, Fig. 5d exhibits the discharge capacities of hollow $NiCo_2O_4$ crossed nanocube electrode against different current rates from 50 $mAhg^{-1}$ to 1000 $mAhg^{-1}$, and each sustained for 50 cycles. The stable cyclic performance is obtained for all rates. A specific capacity of ca. 1060 $mAhg^{-1}$ is recovered when the current rate reduces back to 50 $mAhg^{-1}$ after 100 cycles at higher rates. Fig. 6a and b is the SEM and TEM of hollow $NiCo_2O_4$ crossed nanocubes after 200 cycles at current density of 500 mAg^{-1}, which reveals that the hollow crossed structure of the materials is still kept well without breakage in the process of charge-discharge. The selected area electron diffraction (SAED) pattern is shown as the inset in Fig. 6b, which clearly reveals the presence of cubic NiO and Co_3O_4. The (1 1 1) and (2 0 0) planes of cubic NiO (JCPDS card No. 47-1049), and (3 1 1) and (2 2 2) planes of cubic Co_3O_4 (JCPDS card No. 42-1467) are seen through their inter-planner spacing. These results prove the electrochemical reactions of discharge/charge process mentioned above are reasonable. Compared with the previous reported Ni-Co-O materials,[27-29, 36-41] The material reported here is very attractive due to its facile, fast, and improved lithium storage. The unique hollow structures can shorten the length of Li-ion diffusion, which is benefit for the rate performance. The hollow structure offers a sufficient void space, which sufficiently alleviates the mechanical stress caused by volume change. The multi-elements characteristics of active material allow the volume change to take place in a stepwise manner during electrochemical cycle. Therefore, the hollow $NiCo_2O_4$ crossed nanocube electrode exhibits excellent electrochemical performance.

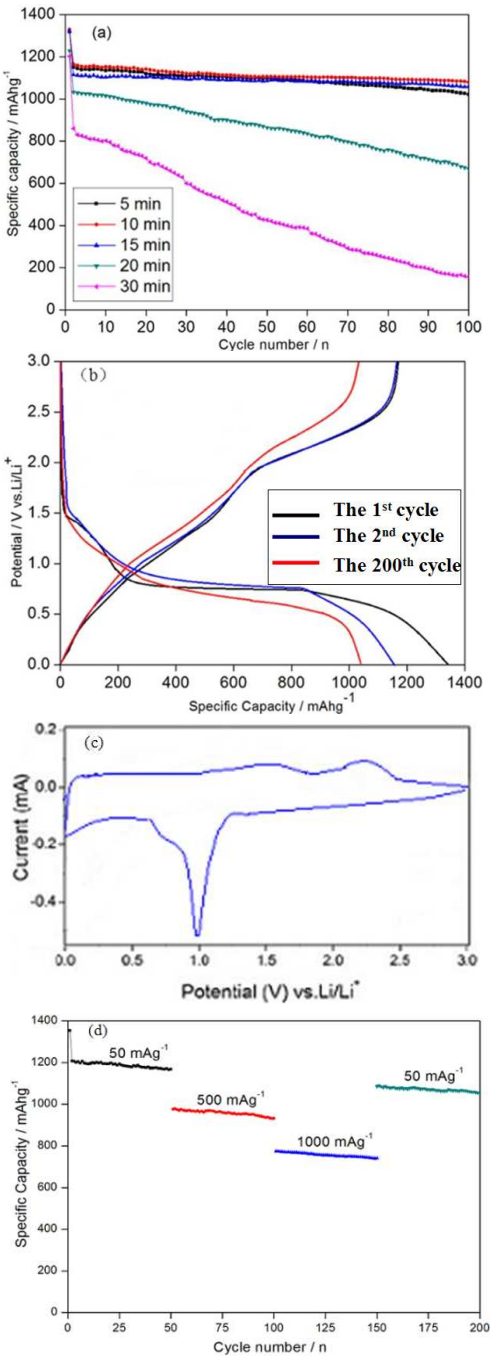

Fig. 5 Electrochemical performance of prepared hollow crossed $NiCo_2O_4$ nanocube electrode: (a) cycling performance of $NiCo_2O_4$ materials with different time of coordinating etching reaction from 5 min to 30 min at constant current density of 100 mAg^{-1}. (b) charge/discharge curves of $NiCo_2O_4$ (10 min) electrode for the 1st, 2nd, and 200th cycle at current density of 200 mAg^{-1}. (c) the first cycle CV curve with a scan rate of 0.05 mVs^{-1}. (d) Rate capability of $NiCo_2O_4$ electrode from 50 mAg^{-1} to 1000 mAg^{-1} for 50 cycles. Electrode potential range of 0.01-3.0 V vs. Li/Li^+.

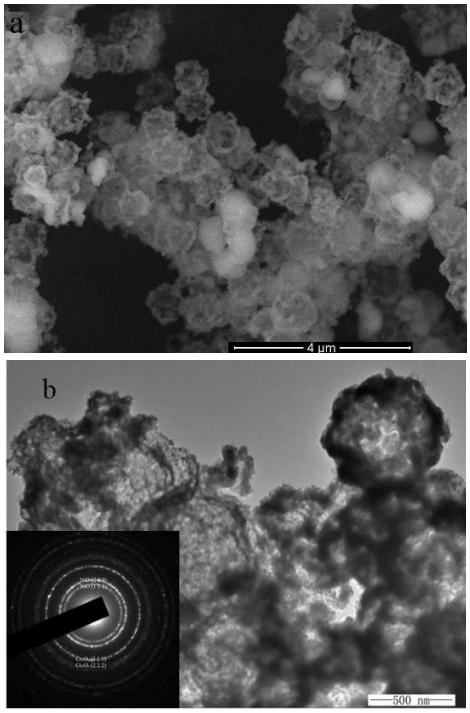

Fig. 6 TEM (a) and TEM (b) image of hollow $NiCo_2O_4$ crossed nanocube electrodes after 200 cycles at current density of 500 mAg^{-1}. The inset in (b) is the selected area electron diffraction (SAED), which clearly reveals the presence of cubic NiO and Co_3O_4. The (1 1 1) and (2 0 0) planes of cubic NiO (JCPDS card No. 47-1049), and (3 1 1) and (2 2 2) planes of cubic Co_3O_4 (JCPDS card No. 42-1467) are seen through their inter-planner spacing.

Conclusions

Hollow crossed $NiCo_2O_4$ nanocubes are successfully synthesized by a facile and fast benign procedure combining with simultaneous coordinating etching reaction and subsequent calcinations. The thickness of shell is ca. 40 nm. The stable reversible capacity of electrode is 1160 $mAhg^{-1}$ and can be retained at 1058 $mAhg^{-1}$ after 200 cycles with the retention of 91.1%. This strategy is simple, cheap and mass-productive, which may shed light on a new avenue for fast synthesis of hollow or amorphous structural nano/micro-functional materials for energy storage, sensor, catalyst, and other new applications.

Acknowledgements

The authors would like to acknowledge financial support provided by Major state basic research development program of China (973 Program, No. 2014CB643406).

Notes and references

School of Chemistry Science and Engineering, Yunnan University, Kunming 650091,Yunnan, China. Fax: +86-871-65036626; Tel: +86-871-65032180; E-mail: guohongcom@126.com

Electronic Supplementary Information (ESI) available: [details of any supplementary information available should be included here]. See DOI:10.1039/b000000x/

1 J. Liu, S. Z. Qiao, S. B. Hartono and G. Q. M. Lu, *Angew. Chem.* 2010, **122**, 5101.
2 B. Wang, J. S. Chen, H. B. Wu, Z. Y. Wang and X. W. Lou, *J. Am. Chem. Soc.* 2011, **133**, 17146.
3 Z. F. Bian, J. Zhu, J. G. Wang, S. X. Xiao, C. Nuckolls and H. X. Li, *J. Am. Chem. Soc.*, 2012, **134**, 2325.
4 X. W. Lou, C. M. Li and L. A. Archer, *Adv. Mater.*, 2009, ***21***, 2536.
5 H. Guo, D. Tian, L. Liu, Y. Wang, Y. Guo and X. Yang, *J. Solid State Chem.*, 2013, **201**, 137.
6 Y. Yin, R. M. Rioux, C. K. Erdonmez, S. Hughes, S, G. A. Somorjai and A. P. Alivisatos, *Science.* 2004, **304**, 711
7 L. Liu, Y. Guo, Y. Peng, X. Yang, S. Wang and H. Guo, *Electrochim. Acta*, 2013, **114**, 42.
8 Q. Zhang, I. Lee, J. B. Joo, F. Zaera and Y. Yin, *Acc. Chem. Res.* 2013, 2013, **46**, 1816.
9 Y. Yao, M. T. McDowell and I. Ryu, *Nano lett.* 2011, **11**, 2949.
10 H. Guo, R. Mao, D. Tian, W. Wang, X. Yang and S. Wang, *J. Mater. Chem. A*, 2013, **1**, 3652.
11 X. Lai, J. Li, B. A. Korgel, Z. Dong, Z. Li, F. Su, J. Du and D. Wang, *Angew. Chem. Int. Ed.* 2011, **50**, 2738.
12 H. Guo, Y. Guo, L. Liu, T. Li, W. Wang, W. Chen and J. Chen, Green Chem., 2014, DOI: 10.1039/C4GC00065J.
13 M. Yang, J. Ma, C. L. Zhang, Z. Z. Yang and Y. F. Lu, *Angew. Chem.* 2005, **117**, 6885.
14 W. Wang, Y. Guo, L. Liu, S. Wang, X. Yang and H. Guo, *J. Power Sources,* 2014, **245**, 624.
15 H. Guo, Y. He, Y. Wang, L. Liu, X. Yang, S. Wang, Z. Huang and Q. Wei, *J. Mater. Chem. A*, 2013, **1**, 7494.
16 C. Wu, X. Wang and L. Zhao, *Langmuir*, 2010, **26**, 18503.
17 H. Guo, L. Liu, Ti. Li, W. Chen, Y. Wang and W. Wang, *Chem. Commun.*, 2014, **50**, 673.
18 Y. Wang, F. Su and J. Y. Lee, *Chem. Mater.* 2006, **18**, 1347.
19 J. Deng, C. Yan and L. Yang, *Nano*, 2013, **7**, 6948.
20 F. Teng, T. Xu, S. Liang, G. Buergen, W. Yao and Y. Zhu, *Catal. Commun.*, 2008, **9**, 1119.
21 H. Guo, W. Wang, L. Liu, Y. He, C. Li and Y. Wang. *Green Chem.*, 2013, **15**, 2810.
22 L. Zhou, D. Zhao and X. W. Lou, *Adv. Mater.,* 2012, **24**, 745.
23 Z. Wang, Z.Wang, W. Liu, W. Xiao and X. W. Lou, *Energy Environ. Sci.*, 2013, **6**, 87.
24 F. Y. Cheng, H. B. Wang, Z. Q. Zhu, Y. Wang, T. R. Zhang, Z. L. Tao and J. Chen, *Energy Environ. Sci.*, 2011, **4**, 3668..
25 F. M. Courtel, H. Duncan, Y. Abu-Lebdeh and I. J.Davidson, J. *Mater. Chem.*, 2011, **21**, 10206.
26 L. L. Li, S. J. Peng, Y. L. Cheah, J. Wang, P. F. Teh, Y. W. Ko, C. L. Wong and M. Srinivasan, *Nanoscale*, 2013, **5**, 134.
27 B. Cui, H. Lin, J. B. Li, X. Li, J. Yang and J. Tao, *Adv. Funct. Mater.*, 2008, **18**, 1440.
28 T. Y. Wei, C. H. Chen, H. C. Chien, S. Y. Lu and C. C. Hu, *Adv. Mater.*, 2010, **22**, 347.
29 L. Li, Y. Cheah, Y. Ko, P. Teh, G. Wee, C. Wong, S. Peng and M. Srinivasan, *J. Mater. Chem. A*, 2013, **1**, 10935.
30 F. Jiao, A. H. Hill, A. Harrison, A. Berko, A. V. Chadwick and P. G. Bruce, *J. Am. Chem. Soc.*, 2008, **130**, 5262.
31 J. F. Ye, H. J. Zhang, R. Yang, X. G. Li and L. M. Qi, *Small*, 2010, **6**, 296.
32 X. W. Lou, Y. Wang, C. Yuan, J. Y. Lee and L. A. Archer, *Adv. Mater.*, 2006, **18**, 2325.
33 Z. Y. Wang, L. Zhou and X. W. Lou, *Adv. Mater.*, 2012, **24**, 1903..
34 H. Guo, Y.P. Wang, W. Wang, L.X. Liu, Y.Y. Guo, X.J Yang, S.X Wang, *Part.Part.Syst.Charact.*, 2013, DOI:10.1002/ppsc.201300198.
35 P. R. Griffiths and D. J. A. Haseth, Fourier Transform Infrared Spectrometry, *John Wilely & Sons, New York,* 1986.
36 G. Q. Zhang, H. B. Wu, H. E. Hoster, M. B. Chan-Park and X. W. Lou, *Energy Environ.* Sci., 2012, **5**, 9453.
37 G. Zhang and X. W. Lou, *Adv. Mater.*, 2013, **25**, 976.
38 H. Jiang, J. Ma and C. Z. Li, *Chem. Commun.*, 2012, **48**, 4465.
39 H. L. Wang, Q. M. Gao and L. Jiang, *Small*, 2011, **7**, 2454.
40 C. Z. Yuan, J. Y. Li, L. R. Hou, L. Yang, L. F. Shen and X. G. Zhang, *J. Mater. Chem.*, 2012, **22**, 16084.
41 L. L. Li, S. J. Peng, Y. L. Cheah, P. F. Teh, J. Wang, G. Wee, Y. W. Ko, C. L. Wong and M. Srinivasan, *Chem. Eur. J.*, 2013, **19**, 5892.
42 Y. Zou and Y. Wang, *Nanoscale,* 2011, **3**, 2615.
43 M. Armand and J.M. Tarascon, *Nature,* 2008, **451**, 652.
44 Y. F. Yuan, X. H. Xia, J. B. Wu, J.L. Yang, Y.B. Chen and S. Y. Guo, *Electrochem. Commun.,* 2010, **12**, 890.
45 X. Wang, X. Li, X. Sun, F. Li, Q. Liu, Q. Wang and D. He, *J. Mater. Chem.,* 2011, **21**, 3571.
46 Y. C. Qiu, S. H. Yang, H. Deng, L. M. Jin and W. S. Li, *J. Mater. Chem.*, 2010, **20**, 4439.

47 Y. Sharma, N. Sharma, G. V. Subba Rao and B. V. R. Chowdari, *Adv. Funct. Mater.*, 2007, **17**, 2855.
48 Y. J. Mai, S. G. Shi, D. Zhang, Y. Lu, C. D. Gu and J. P. Tu, *J. Power Sources*, 2012, **204**, 155.
49 B. Liu, J. Zhang, X. F. Wang, G. Chen, D. Chen, C. W. Zhou and G. Z. Shen, *Nano Lett.*, 2012, **12**, 3005.
50 S. L. Xiong, J. S. Chen, X. W. Lou and H. C. Zeng, Adv. Funct. Mater., 2012, **22**, 861.